1   Autonomous underwater vehicle based marine multi-component self-potential

2   method: observation scheme and navigational correction

3

4   Zhongmin Zhu[1 2], Jinsong Shen[1], Chunhui Tao[2 3], Xianming Deng[2], Tao Wu[2], Zuofu Nie[1], Wenyi

5   Wang[1], Zhaoyang Su[1].

6   [1]State Key Laboratory of Petroleum Resources and Prospecting, China University of Petroleum

7   (Beijing), Beijing, 102249, China

8   [2]Second Institute of Oceanography, Ministry of Natural Resources, Hangzhou 310012, Zhejiang,

9   China

10   [3] School of Oceanography, Shanghai Jiaotong University, Shanghai 200030, China

11

12   **Corresponding author:** Jinsong Shen (shenjinsongcup@163.com);

13   Chunhui Tao (taochunhuimail@163.com)

Abstract

15   Marine self-potential (SP) investigation is an effective method to study deep-sea hydrothermal vents

16   and seafloor sulfide deposits. At present, one of the commonly used marine self-potential system is a

17   towed array of electrodes. Large noises are recorded when great change of electrode distance and array

18   attitude occur due to the complex seafloor topography. In this paper, a new multi-component electric

19   field observation system based on underwater autonomous underwater vehicle (AUV) was introduced

20   for the measurement of seafloor self-potential signals. The system was tested in a lake and the multi-

21   component self-potential data were collected. Observed data involve the navigational information of

22   AUV, which could be corrected using a rotation transform. After navigational correction, measured

23   data can recover the location of the artificial source using self-potential tomography. The experimental

24   results showed that the new SP system can be applied to marine SP observations, providing an efficient

25   and low-noise SP acquisition method for marine resources and environmental investigations.

26   **Keywords:** Underwater self-potential method; Autonomous underwater vehicles; Rotation correction;

27   Multi-component inversion;

28

Introduction

30   Self-potential (SP) method has a long history on land and plays an important role in the delineation

31   and resource evaluation of metal sulfide ore bodies (Fox, 1815). It is generally believed that the

32   negative anomaly of SP is related to the metal sulfide ore bodies (Sato and Mooney, 1960; Corry, 1985;

33   Naudet and Revil, 2005; Komori et al., 2017). In view of the great difference between the marine and

34   the land environments, geophysical methods are still not economical and efficient enough, which limits

35   the exploration of marine resources. With the development of electronic instruments as well as the

36   better understanding of the mechanism of SP response, the application of SP exploration has been

37   gradually developed from land prospecting to shallow water and deep-sea exploration of polymetallic

38   sulfide (Corwin, 1973; Corwin, 1976; Tao et al., 2013). In addition to mineral exploration, the

39   underground water flow driven by seafloor thermal activity and thermal gradient will also produce

40   detectable SP anomalies. SP measurement method has also been applied to study the geothermal and

41   hydrothermal activity of deep seafloor (Heinson, 1999). Eppelbaum（Eppelbaum, 2019）introduced

42   a new parameter into SP interpretation -'self-potential moment', and this method has been effectively

43   applied at several ore deposits in the South Caucasus.

44   In 1973, Corwin (Corwin, 1973) began to develop the marine SP detection system, and in 1976, an SP

45   anomaly around 300 mV was discovered which related with the offshore extensions of sulfide deposit

46 (Corwin, 1976). In 2000, Sudarikov and Roumiantsev conducted SP and Eh (oxidation reduction

47 potential) survey at Logatchev hydrothermal vent in Mid-Atlantic ridge, and inferred the spatial

48 distribution characteristics of hydrothermal plume near the vent (Sudarikov and Roumiantsev, 2000).

49 Cherkashev (Cherkashev et al., 2013) used a deep-towed SP instrument to locate seafloor sulfide

50 deposits associated with hydrothermal vents near the mid-Atlantic ridge. Kawada and Kasaya (Kawada

51 and Kasaya, 2017, 2018) also observed negative SP anomalies and associated hydrothermal sulfide

52 deposits in the Izena hydrothermal field of the Okinawa trough in Japan by using the deep-sea towed

53 SP array. Safipour (Safipour et al., 2017) mounted SP electrodes on transient electromagnetic

54 equipment and detected SP negative anomaly over inactive sulfide at Tyrrhenian Sea.

55 The configuration described above connects the electrode array by a cable or insulated elastic rod,

56 which is easy to operate in marine environment. However, there are also several inconveniences with

57 soft-connected towed SP arrays. The towed array is susceptible to be distorted by ocean currents, and

58 the distance between the soft-connected electrodes changes greatly, both of which will affect the

59 precision of the measured SP amplitude, especially in mid-ocean ridges, where the seafloor topography

60 varies greatly (Constable et al., 2018).

61 To improve the stability and efficiency of marine SP configuration used in the deep-sea environment,

62 combined with the ideas of Constable et al. (2018), the autonomous underwater vehicle (AUV) was

63 modified with four channel electric field sensors in the tail to detect the marine SP responses (shorted,

64 AUV-SP), which was expected to be helpful for seafloor sulfide exploration. To test the stability and

65 determine the influencing factors, two AUV experiments were conducted during the July of 2019 at

66 Qiandao Lake in eastern China. The water depth is about 40 m, and there was little artificial

67 interference around the test site, making it an ideal place to test the new system and analyze the electric

68 field noise. The main purpose of the AUV-SP system test was: i) to investigate the optimized position

69 of SP electrode on AUV to minimize the interference of noises from the AUV; ii) to verify the

70 validation of developed system by using the known artificial current source. In addition, measured

71 multi-component data were inverted using self-potential tomography (Jardani et al., 2008; Revil et al.,

72 2008; Rittgers et al., 2013) to verify the capability of multicomponent self-potential detection.

73

74 ## 1. AUV-based SP system

75 SP measurement system mainly consists two parts, i.e. electric field sensors (Ag-AgCl non-polarizing

76 electrodes) and data logger chamber. The electronic circuit of the data logger was encapsulated in the

77 pressure chamber, which was mounted on the back of the AUV with a diving capacity of 4500 m. The

78 electric field sensors and two orthogonal extension rods of 2 m were arranged horizontally and

79 vertically at the tail of AUV (Figure 1). The electrode1 and 2 were fixed at the end of the horizontal

80 extension rod along the moving direction of AUV to measure inline component of the electric field E_R.

81 The electrode 5 and 6 were attached on the end of vertical extension rod to measure the vertical

82 component E_V. The electrode 3 and 4 were mounted on the left and right sides of the abdomen of AUV

83 to measure the horizontal component orthogonal to the AUV E_T. The E_T data for electrodes on surface

84 of AUV were affected by propulsion motor and short electrode space (less than 30cm), leading a larger

85 noise level than the rear electrodes. The component E_T were greatly distorted; thus, the followed data

86 processing and analysis will focus on E_R E_V.

87 The installation of the SP receivers did not affect the data flow or function of other sensors mounted

88 on AUV including magnetic field sensor, sonar, underwater cameras and other plume detective sensors.

89 Navigation system consists ultra-short baseline, depth sensor and attitude orientation (Wu et al., 2019).

2. Lake test design and data acquisition of AUV based SP system

2.1 Noise levels and observation design

There are different disturbances appearing in the SP detection, including natural noises and artificial noises (Eppelbaum, 2020). The electrodes are calibrated in the laboratory, and the potential difference between the electrode pairs is less than 0.1 mV. Therefore, the main factors affecting the SP signal on AUV were as follows: electrode dipole length, the stability of the observation system and the interference to the electrodes from the AUV body (batteries, thrusters, etc.). The signal of natural electric field in deep seawater was very weak, and the measured magnitude of electric potential difference was in direct proportion to the electrode dipole length. Large dipole length should be used for weak signal, and the electrode dipole length should be increased as much as possible without affecting the normal navigation of AUV. The dipole length in the lake test was preset as 2 m.

Considering the interference of the electrode by the AUV power supply device, a pair of electrodes were placed on the surface of the AUV, and the other two groups of electrodes were installed at the tail of the AUV with the hard-connecting rod as a bracket, as far as possible away from the AUV body. The reason for choosing the hard-connecting rod was to keep the electrode distance constant when the submersible moves underwater which is very important in the marine SP detection, because the soft link rod would be distorted by bottom current of seawater when AUV moves near the seafloor and therefore would not be suitable. Changing of electrode distance will introduce the attitude deformation noise and strongly affect the recorded signals especially when the electrode distance is small.

2.2 Equipments used for the test

As for the materials of hard-connecting rod to connect the electrodes, on the one hand, non-magnetic materials should be used to minimize the influence on the fluxgate magnetometer at the tail of the

112   submersible; On the other hand, the connecting rod should be insulated to electric current to minimize

113   the induced electric field generated by cutting the earth magnetic field during the movement of AUV.

114   The electrode bracket used in the lake test was made of PVC material without magnetic components

115   and fully insulated. These conditions meet the above requirements.

116   *2.3 Layout of artificial SP source*

117   The test of the AUV based SP system was conducted at a testing platform, in the center of Qiandao

118   Lake. According to the classic geo-battery model (Sato and Mooney, 1960), SP anomalies generated

119   by the geo-battery mechanism are expected to be dipolar in nature and the SP source can be equivalent

120   to electric dipole source (see also Naudet and Revil, 2005, for biogeobatteries). To verify the

121   effectiveness of AUV-SP system, an artificial diploe source was set up as shown in Figure 2 Firstly, a

122   100 m nylon rope was mounted on an insulating float for fixing test platform, and four buoys were

123   attached to the rope to make it float on the surface of the water. Positive and negative electrodes were

124   extended by wires, which were fixed along the rope into the lake. The distance between the positive

125   and negative poles was about 56 m. The 36 V DC power generator was placed in the platform. Copper

126   plates were attached in the positive and negative terminals, respectively, to reduce the voltage

127   attenuation and increase the conductive area of the current electrodes. The power supply provides a

128   constant voltage about 36 V, the electric potential on the positive pole and the negative pole is 18 V

129   and -18 V, respectively, when ignore the difference of copper plates. These electric potentials are also

130   used in the subsequent numerical simulations.

131   *2.4 Data acquisition*

132   Before the AUV entered the water, all electrodes were placed on the AUV system as shown in Figure

133   1. The AUV first dived to 8 m depth at a constant speed, and performed repeated measurements

134 surrounding the positive and negative poles. The average speed of the AUV was about 1 knot (0.5 m/s),

135 and the sampling frequency of the electric field sensors were 150 Hz. Other tests including repeatedly

136 switching on and off manual power, changing navigation speed and steering were also conducted to

137 determine the influence of AUV body on the electric field signal during navigation.

138

139 ## 3. Results and analysis

140 *3.1 Noise analysis of the lake test*

141 Sensors mounted on AUV do not move with waves, we detect obvious anomaly around active

142 source and noises from AUV are analyzed in this section. Figure 3 shows the three-component electric

143 field in water. The artificial source produced a stable electric field similar to an electric dipole source

144 in water. At the beginning of the test, the system was far away from the negative pole, and the collected

145 electric field was approximately equal to the background field. The amplitude fluctuated around 0 mV.

146 When passing near the location of the artificial current source, the electric field sensor could detect

147 that the potential changed up to 30 mV. Because the system was always close to the negative electrode

148 during the measurement process, the recorded electrical field was less affected by the positive

149 pole/electrode.

150 In order to analyze the influence of AUV body on the electric field sensor, the frequency spectrum of

151 the electric field time series measured by the artificial current source was analyzed (We calculate the

152 power spectrum of time series and convert the unit in dB by using 10log10(power)). Figure 4 shows

153 the time series data of the three-component electric field for 15 min. The overall noise level was related

154 to the position of the electrode. Results of power spectrum calculation showed the following

155 characteristics:

156 1) The effective signal was mainly concentrated in the low frequency, and the noise level decreased

157 with the increase of frequency;

158   2)   The electrodes far from the AUV body had lower noise;

159   3)   The noise of vertical component was lower than that of horizontal one;

160   4)   Except for the 50 Hz industrial interference, the peak values of the power spectrum were basically

161   consistent with the rotation speed of propellers (The 1.4 Hz corresponds to the speed of 85 turns/min,

162   the peaks of 3.5 - 4.5Hz corresponds to the speed from 210- 285 turns/min).

163   In addition, the noise of 2.1 Hz corresponding to the vertical component was mainly caused by the

164   vibration of the connecting rod in the water. The camera attached to the head of the connecting rod

165   recorded the corresponding vibration image, providing a reference for improving the material and

166   installation mode of the connecting rod.

167   *3.2 AUV navigation attitude impact and correction*

168   The attitude of AUV has a significant impact on the SP data, therefore should be considered and

169   corrected in the field data processing and interpretation. The attitude angle in the local coordinate

170   system is usually used to describe the attitude and spatial position of AUV, including azimuth angle

171   (heading), pitch angle and roll angle. The global reference coordinate system was determined

172   according to the geodetic coordinates and the position of the survey lines. Then the relative relationship

173   between the two coordinates was determined by the rotation of the coordinate system as shown in

174   Figure 5c. The coordinate axis of the reference coordinate system is assumed as (X_0, Y_0, Z_0). The

175   local coordinate system of the first rotation (X_1, Y_1, Z_1) is obtained by rotating the azimuth angle H

176   clockwise with Z_0 as the rotation axis, then (X_2, Y_2, Z_2) is obtained by rotating pitch angle P

177   clockwise with X_1 as the rotation axis, and finally (X_3, Y_3, Z_3) is obtained by rotating the roll angle

178   R clockwise along Y_2 axis. The above procedure can be represented by three rotation matrices

179   below. The electric field supposed to be rotated in the reference coordinate system is $\mathbf{E}_g(E_x, E_y, E_z)$,

180   and the measured electric field in the local coordinate system after rotation is $\mathbf{E}_{rot}(E_R, E_T, E_V)$, then

181    $E_{rot} = RY \cdot RX \cdot RZ \cdot E_g$, in component form we have:

182
$$\begin{bmatrix} E_R \\ E_T \\ E_V \end{bmatrix} = \begin{bmatrix} \cos R & 0 & -\sin R \\ 0 & 1 & 0 \\ \sin R & 0 & \cos R \end{bmatrix} \begin{bmatrix} 1 & 0 & 0 \\ 0 & \cos P & \sin P \\ 0 & -\sin P & \cos P \end{bmatrix} \begin{bmatrix} \cos H & \sin H & 0 \\ -\sin H & \cos H & 0 \\ 0 & 0 & 1 \end{bmatrix} \begin{bmatrix} E_x \\ E_y \\ E_z \end{bmatrix} \quad (1)$$

183   The corresponding inverse transformation is:

184    $$E_g = (RY \cdot RX \cdot RZ)^{-1} E_{rot} = RX^T \cdot RZ^T \cdot RY^T E_{rot} \quad (2)$$

185   The AUV takes such actions as obstacle avoidance and steering according to the change of bathymetry

186   when navigating over the seafloor. The electric field $\mathbf{E}_{obs}$ recorded by the sensors attached to the AUV

187   contains information of the navigation attitude. By ignoring acquisition noise and positioning error,

188    $\mathbf{E}_{obs}$ recorded by AUV should be consistent with the rotated $\mathbf{E}_{rot}$. It can be verified whether the

189   measured electric field of AUV is consistent with the electric field generated by dipoles in uniform

190   space through numerical simulation.

191   Based on the situation of the lake test, a three-dimensional (3D) model of 100×100×30 m was

192   established in Cartesian coordinate system, where positive and negative poles of the dipole were

193   located at (3, 75, -1) and (54, 80, -0.5), respectively. The 3D model was discretized into unstructured

194   grids; the Poisson equation of steady-state current field was solved by the finite element method; and

195   boundary conditions of the first kind were used at the bottom of the lake. The global electric field

196    $\mathbf{E}_g(E_x, E_y, E_z)$ was extracted according to AUV location data, and then the electric field in the local

197   coordinate system along the direction of profile denoted as $\mathbf{E}_{rot}(E_R, E_T, E_V)$ was calculated using

198   Eq.(1). Field data measured by the AUV were denoted as $\mathbf{E}_{obs}(E_R, E_T, E_V)$. The relationship between

199   global $\mathbf{E}_g(E_x, E_y, E_z)$ and local $\mathbf{E}_{rot}(E_R, E_T, E_V)$ is shown in Figure 5b. When AUV is moving from

200   south to north, the observation field is in the same direction as the reference field, and opposite as

201   AUV moving from north to south.

202   The attitude of AUV is shown in Figure 6a. AUV navigated stably in the lake and the roll angle was

203   less than 5°. Pitch changed when vehicle was rising or falling and the overall pitching angle was less

204   than 20°. In the measured range shown in Figure 6a, the vehicle changed direction twice at 02:11 and

205   02:14, respectively. The measured and simulation results in Figure 6b and Figure 6c showed that the

206   attitude of the AUV has different impacts on each components of the electric field. Specifically, the

207   azimuth has significant influence on the horizontal component of the electric field, but has little

208   influence on the vertical component. When the survey line went along SW direction, variation trend

209   of $\mathbf{E}_R$ along the survey line (red solid line in Fi. 6b) and global component $\mathbf{E}_x$ was in the opposite;

210   when the survey line went along northeast (NE) direction, $\mathbf{E}_R$ and $\mathbf{E}_x$ changed in the same direction.

211   After rotation correction, the observation data of the submersible were basically consistent with the

212   simulation results. The position where the gradient of the horizontal electric field component changed

213   the most significantly, corresponded to the negative pole of the artificial source. Azimuth has little

214   effect on the vertical component, because the AUV was always below the negative source and the

215   electric field direction pointed up. Therefore, the change of azimuth angle will not change the direction

216   of the vertical component. In addition, because that the pitch angle was very small, and the attached

217   electrode was basically maintained in the vertical state, the vertical component of the measured electric

218   field $\mathbf{E}_V$ was approximately equal to that of the global component $\mathbf{E}_Z$.

219

220   ## 4. Inversion Scheme of AUV based self-potential data

221   The forward problem of SP can be expressed by Poisson equation of potential (Jardani et al.,2008):

222
$$\nabla \cdot (\sigma \nabla V) = \nabla \cdot \mathbf{J}_s = \Im$$
$$\mathbf{E} = -\nabla V$$
(3)

223 where $\Im$ is the volumetric current density (A/m^3), $\mathbf{J}_s$ is the current density vector (A / m^2), σ is the

224 conductivity (S/m), $\mathbf{E}$ is the electric field vector, and V represents the SP field.

225 By changing the source term of Eq. (3), the SP response to various effects can be calculated, such as

226 the flow potential related to groundwater flow (Ahmed et al., 2013) or the geo-battery model related

227 to polymetallic deposits (Rittgers et al., 2013).

228 In order to investigate the reliability and interpretability of electric field data measured by the AUV-

229 SP system, the regularized least square method was applied for the inversion of the artificial SP source.

230 Assuming that $\boldsymbol{m}$ is the bulk current density model vector and $\boldsymbol{m_0}$ is the reference model, the

231 inversion can be expressed as the minimization of the following objective function：

232 $$\phi(\boldsymbol{m}) = \left\| \mathbf{W_d}\Delta\boldsymbol{d} \right\|^2 + \alpha \left\| \mathbf{W}(\boldsymbol{m} - \boldsymbol{m_0}) \right\|^2 \qquad (4)$$

233 where $\mathbf{W_d}$ is the data weighting matrix, $\Delta\boldsymbol{d}$ is the difference between the data $\boldsymbol{d}$ obtained by

234 forward modeling and the observed data $\boldsymbol{d}^{obs}$, also known as data residual. Here, the measured electric

235 field component was selected as the observation data, $\mathbf{W}$ is the model weighted diagonal matrix, and

236 α as the regularization factor. Regularization factor α was used to balance the model constraints

237 and data fitting function in the process of solving the model. It can be determined by L-curve criterion

238 or GCV method, or by experience. Because the electric field decays rapidly with distance, the inversion

239 of seafloor SP data only gives a shallow current density distribution, which cannot accurately reflect

240 the situation of space current dipole source under the seafloor. Therefore, it is necessary to introduce

241 depth weighting function to enhance the sensitivity of grid element far from the observation point. The

242 depth weighting function $\mathbf{W_z}$ should be placed in the model constraints as follows (Biswas and

243 Sharma, 2017; Portniaguine and Zhdanov, 1999):

244 $$W_j = (\sum_{i=1}^{N} (J_{ij})^2)^{p/4}, j = 1,...,M \qquad (5)$$

245 where W_j is the jth element on the main diagonal of matrix $\mathbf{W_z}$, $\mathbf{J}$ is the sensitivity matrix (or

246 Jacobian matrix). M is the number of model vector elements; N is the number of the observation point.

247 p is constant, generally equals to 1. The extent of depth weighting can be adjusted by the value of p.

248 For multi-component inversion, the full three electric field were used and the total number of

249 observation data became 3*N.

250 In application, the SP data can be inverted in many ways to determine the flow direction of the fluid

251 or the location of the self-potential source. When the source location is to be solved, it was usually

252 assumed that the conductivity distribution in the space is known or determined by other electrical

253 exploration methods (DC conductivity or induction-based electromagnetic methods), then the SP

254 source can be equivalent to the external current source. Therefore, this study used the inverted

255 volumetric current density distribution to locate the simulated artificial source. On land, SP method

256 usually directly measures the electric potential between the roll electrode and a fixed electrode,

257 therefore, the potential data V is directly chosen for inversion. However, in the marine environment, it

258 is impossible to fix a reference electrode on the seafloor when the ship or AUV is moving. Therefore,

259 the SP method conducted in the marine environment usually measures the gradient of electric potential,

260 that is the electric field, and the potential is calculated indirectly by numerical integration. In the case

261 of this study, the measured multi-components electric field components were directly inverted.

262 Owing to the limited observation data collected by AUV-SP system near the artificial source, the

263 inversion result is nonunique. Therefore, the constraints of known information such as the lake water

264 conductivity (1 S/m, measured with the environment sensor from AUV) and lake bottom sediment

265 conductivity (assumed as 0.1 S/m) were added to the inversion. To investigate the advantages of multi-

266 component inversion, single component and two component observation data were used for inversion

267 and the inversion results were compared. Figure 7. shows the results obtained by inversion of electric

268 field data of single component (horizontal component, vertical component, respectively) and two

269 components (horizontal component and vertical component) under the same constraint conditions.

270 Negative charge density was recovered surrounding the negative pole of the artificial source in all

271 results, which preliminarily revealed the reliability of the system and the effectiveness of the inversion

272 method. Indeed, cause the AUV-SP system's navigation path in the lake is mainly near the negative

273 pole of the artificial source, the negative pole position of the artificial source can be precisely located

274 while positive pole is not well-located due to the lack of observation data of surrounding area, although

275 some positive charge density is retrieved along the survey line. By comparing the inversion results

276 between single component (Figure 7a and b) and multi-component (Figure 7c), it was observed that

277 the inversion results of the two horizontal components of the electric field were more focused, and the

278 negative charge intensity was concentrated, while the negative charge density obtained from the

279 inversion results of the single vertical component of the electric field was accompanied by positive

280 charge anomaly, which dispersed the negative charge energy, and deviated from the actual situation.

281 Combination of vertical and horizontal components of electric field data restricts the horizontal

282 distribution of charge density and makes the inversion more consistent with the actual artificial source.

283 In addition, the current flow direction (Figure 7b, d, f) also exhibits that the inversion of only one

284 single component will produce wrong current direction, more additional constraints (e.g. boundary

285 limits, heterogeneous distribution of conductivity) were required to obtain reasonable inversion results.

286 Therefore, multi-component detection of electric field is necessary when addressing complex

287 geological structure especially involving flow of fluids.

5. Conclusion

A seafloor SP measurement system which consisted of three pairs of perpendicular electrodes attached to the AUV (Qianlong 2) was introduced. By deploying an artificial current source, the multi-component electric field responses in the water were measured by AUV in Qiandao Lake. The observed results were consistent with the numerical simulation, which verifies the feasibility of the AUV-SP system for multi-component SP exploration. At present, the AUV-SP system can work in water for about 40 hours, and complete the SP measurement of high-resolution area of about 20 km^2.

The test results of two surveys showed that the AUV-SP system has good consistency and repeatability, and the overall noise level of the measured data is relatively low, which meets the requirements of near seafloor SP exploration in large scale. The inversion of the test data of AUV-SP system demonstrated that the position and intensity of the inverted current source were basically consistent with the actual position and intensity of the artificial current source. Therefore, the SP response measured by AUV-SP system can be used to locate the seafloor SP source, so as to achieve the exploration and evaluation of the seafloor sulfide deposits. In the case of simple geoelectric structure, single vertical component measurement would be sufficient to locate the SP source, but in solving the complex problems such as hydrothermal or fluid flow, three-component SP measurement is crucial.

In view of the vibration noise of the connecting rod presented in this test, our next step will be to select a more suitable material and design a bracket with better rigidity to reduce the vibration noise. The experience and data accumulated in this experiment also provide a reference for the future researches of active source electromagnetic detector on AUV.

Data availability

The raw data from the experiments are available upon request (591149254@qq.com)

310 *Author contributions*

311 ZZ process the data and wrote the paper. JS was the project leader. CT provided ideas and designed

312 the AUV-SP system, XD, TW, ZN and WW together tested the system, ZS proofread the manuscript.

313 **Competing interests**

314 The authors declare that they have no conflict of interest.

315 **Acknowledgements**

318 *Financial support*

322

References:

Ahmed, A. S., Jardani, A., Revil, A., and Dupont, J. P.: SP2DINV: A 2D forward and inverse code for streaming potential problems. Computers & Geosciences, 59, 9-16, https://doi.org/10.1016/j.cageo.2013.05.008, 2013.

Biswas, A., and Sharma, S. P.: Interpretation of self-potential anomaly over 2-D inclined thick sheet structures and analysis of uncertainty using very fast simulated annealing global optimization, Acta Geodaetica et Geophysica, 52, 439-455, https://doi.org/10.1007/s40328-016-0176-2, 2017.

Cherkashev, G. A., Ivanov, V. N., Bel Tenev, V. I., Lazareva, L. I.,Rozhdestvenskaya, I. I., Samovarov, M. L., Poroshina, I. M., Sergeev, M. B., Stepanova, T. V., and Dobretsova, I. G.,: Massive sulfide ores of the northern equatorial Mid-Atlantic Ridge, Oceanology, 53, 607-619, https://doi.org/10.1134/S0001437013050032, 2013.

Constable, S., Kowalczyk, P., and Bloomer, S., Measuring marine self-potential using an autonomous underwater vehicle, Geophysical Journal International, 215, 49-60, https://doi.org/10.1093/gji/ggy263, 2018.

Corry, C. E.,: Spontaneous polarization associated with porphyry sulfide mineralization, Geophysics, 50, 1020-1034, https://doi.org/10.1190/1.1441967, 1985.

Corwin, R. F.: Offshore Application of Self-potential Prospecting, Scripps Institution of Oceanography Library, 1973.

Corwin, R. F.: Offshore use of the self-potential method: Geophysical Prospecting, 24, 79-90, https://doi.org/10.1111/j.1365-2478.1976.tb00386.x, 1976.

Eppelbaum, L.V.: Advanced analysis of self-potential field analysis in ore deposits of the South Caucasus, Proceedings of the National Azerbaijan Academy of Sciences, 2, 21-35, DOI: 10.33677/ggianas20190200029, 2019.

Eppelbaum, L. V.: Quantitative analysis of self-potential anomalies in archaeological sites of Israel: an overview. Environmental Earth Sciences, 79, 1-15, https://doi.org/10.1007/s12665-020-09117-w, 2020.

Fox R W.: On the electro-magnetic properties of metalliferous veins in the mines of cornwall. Abstracts of the Papers Printed in the Philosophical Transactions of the Royal Society of London. London, 411-411. 1833

Heinson, G.: Marine self potential exploration: Exploration Geophysics, 30, 1-4, https://doi.org/10.1071/EG999001, 1999.

Jardani, A., Revil, A., Bolève, A. and Dupont, J. P.: Three-dimensional inversion of self-potential data used to constrain the pattern of groundwater flow in geothermal fields, Journal of Geophysical Research, 113, B09204, https://doi.org/10.1029/2007JB005302, 2008.

Kawada Y, Kasaya T. Marine self-potential survey for exploring seafloor hydrothermal ore deposits. Scientific reports, 7(1), 1-12. https://doi.org/10.1038/s41598-017-13920-0, 2017

Kawada, Y., and Kasaya, T.: Self-potential mapping using an autonomous underwater vehicle for the Sunrise deposit, Izu-Ogasawara arc, southern Japan, Earth, Planets and Space, 70, 142, https://doi.org/10.1186/s40623-018-0913-6, 2018.

Komori, S., Masaki, Y., Tanikawa, W., Torimoto, J., Ohta, Y., Makio, M., Maeda, L., Ishibashi, J., Nozaki, T., Tadai, O., and Kumagai, H.: Depth profiles of resistivity and spectral IP for active modern submarine hydrothermal deposits: a case study from the Iheya North Knoll and the Iheya Minor Ridge in Okinawa Trough, Japan, Earth, Planets and Space, 69, 114 https://doi.org/10.1186/s40623-017-0691-6, 2017.

Naudet, V., and Revil, A.: A sandbox experiment to investigate bacteria-mediated redox processes on self-potential signals, Geophysical Research Letters, 32, L11405, https://doi.org/10.1029/2005GL022735, 2005.

Portniaguine, O., and Zhdanov, M. S.: Focusing geophysical inversion images, Geophysics, 64, 874-887, https://doi.org/10.1190/1.1444596, 1999.

Revil, A., Finizola, A., Piscitelli, S., Rizzo, E., Ricci, T., Crespy, A., Angeletti, B., Balasco, M., Barde Cabusson, S., Bennati, L., Bolève, A., Byrdina, S., Carzaniga, N., Di Gangi, F., Morin, J., Perrone, A., Rossi, M., Roulleau, E.,and Suski, B,: Inner structure of La Fossa di Vulcano (Vulcano Island, southern Tyrrhenian Sea, Italy) revealed by high‐resolution electric resistivity tomography coupled with self‐potential, temperature, and CO2 diffuse degassing measurements, Journal of Geophysical Research: Solid Earth, 113, B07207, https://doi.org/10.1029/2007JB005394, 2008.

Rittgers, J. B., Revil, A., Karaoulis, M., Mooney, M. A., Slater, L. D., and Atekwana, E. A.: Self-potential signals generated by the corrosion of buried metallic objects with application to contaminant plumes, Geophysics, 78, EN65-EN82, https://doi.org/10.1190/geo2013-0033.1,

381   2013.

382   Safipour, R., Hölz, S., Halbach, J., Jegen, M., Petersen, S., and Swidinsky, A.: A self-potential

383   investigation of submarine massive sulfides, Palinuro Seamount, Tyrrhenian Sea, Geophysics,

384   82(6), A51-A56, https://doi.org/10.1190/geo2017-0237.1, 2017.

385   Sato, M., and Mooney, H. M.: The electrochemical mechanism of sulfide self-potentials, Geophysics,

386   25, 226-249, https://doi.org/10.1190/1.1438689, 1960.

387   Sudarikov, S. M., and Roumiantsev, A. B.: Structure of hydrothermal plumes at the Logatchev vent

388   field, 14 45′ N, Mid-Atlantic Ridge: evidence from geochemical and geophysical data, Journal

389   of Volcanology and Geothermal Research, 101, 245-252, https://doi.org/10.1016/S0377-

390   0273(00)00174-8, 2000.

391   Tao, C., Xiong, W., Xi, Z., Deng, X., and Xu, Y.: TEM investigations of South Atlantic Ridge 13.2 S

392   hydrothermal area, Acta Oceanologica Sinica, 32, 68-74, https://doi.org/10.1007/s13131-013-

393   0392-3, 2013.

394   Wu, T., Tao, C., Zhang, J., Wang, A., Zhang, G., Zhou, J., and Deng, X.: A hydrothermal investigation

395   system for the Qianlong-II autonomous underwater vehicle, Acta Oceanologica Sinica, 38, 159-

396   165, https://doi.org/10.1007/s13131-019-1408-4, 2019.

397

398 **Figures**
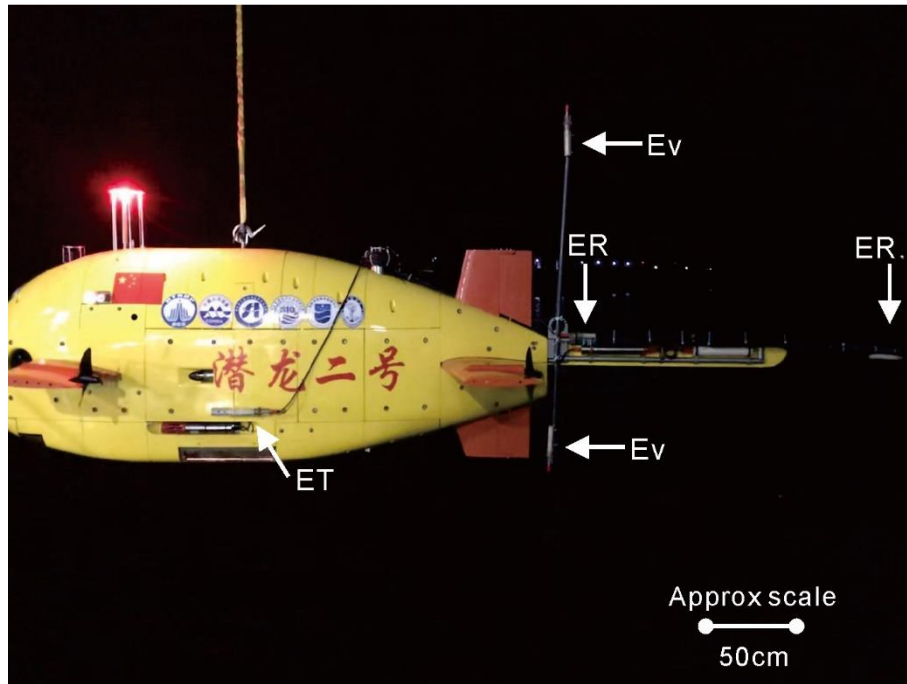
400 **Figure 1** Layout of each channel electrode on AUV. E_R is the inline horizontal component of electric

401 field recorded by channel 1 and 2; E_T is the crossline horizontal component of electric field recorded

402 by channel 3 and 4; E_V is the vertical component of electric field recorded by channel 5 and 6.
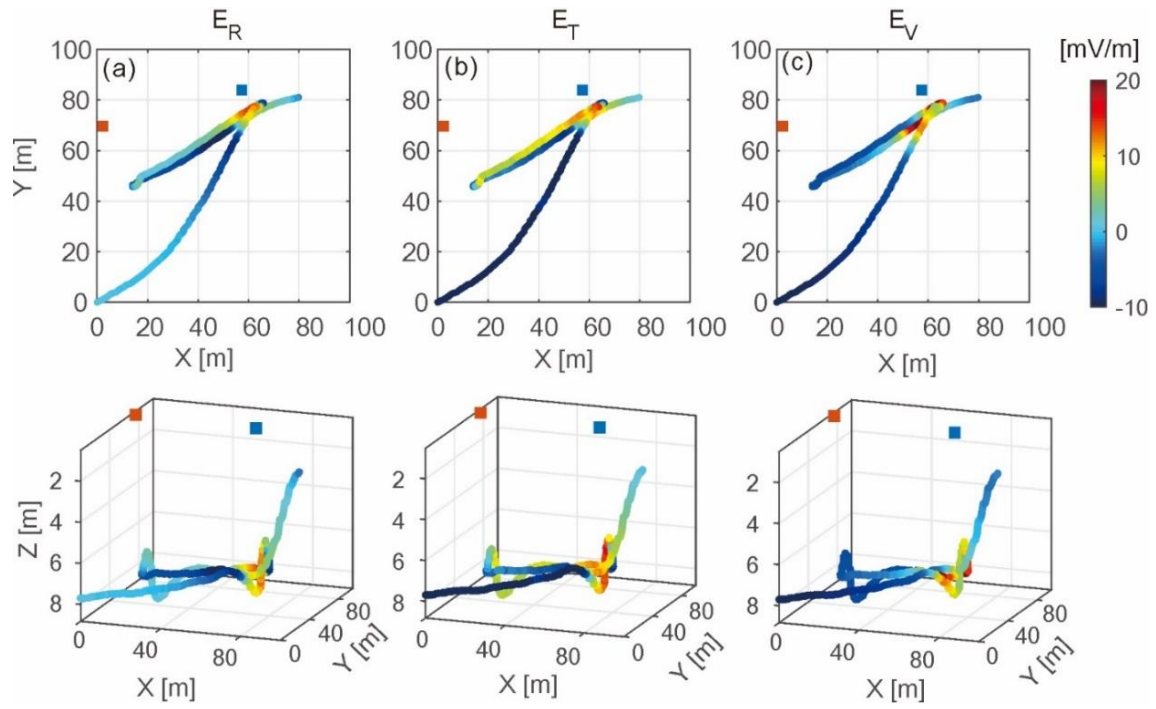
403
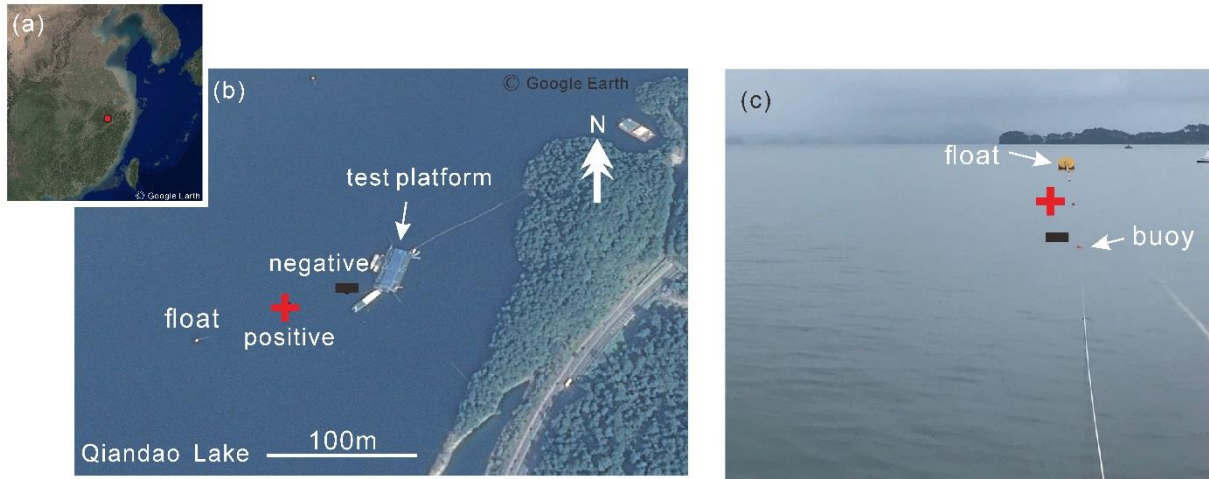
404

405 **Figure 2** Layout of artificial SP source. (a) Location of Qiandao Lake (source: Google Earth, 2019);

406 (b) Position of artificial source in the water (plan view) (source: Google Earth, 2019); (c) Zoom in

407 location of artificial source, red plus and black minus denote the positive and negative poles of the DC

408 power, respectively.

409

Figure 3 The planar distribution of the three components of the electric field measured by AUV based SP system (plan view in the upper panel, 3D view in the lower panel). (a) Inline component of electric field, (b) Crossline component of electric field, (c) Vertical component of electric field; Red and blue dots represent the positive and negative poles of the artificial source, respectively.
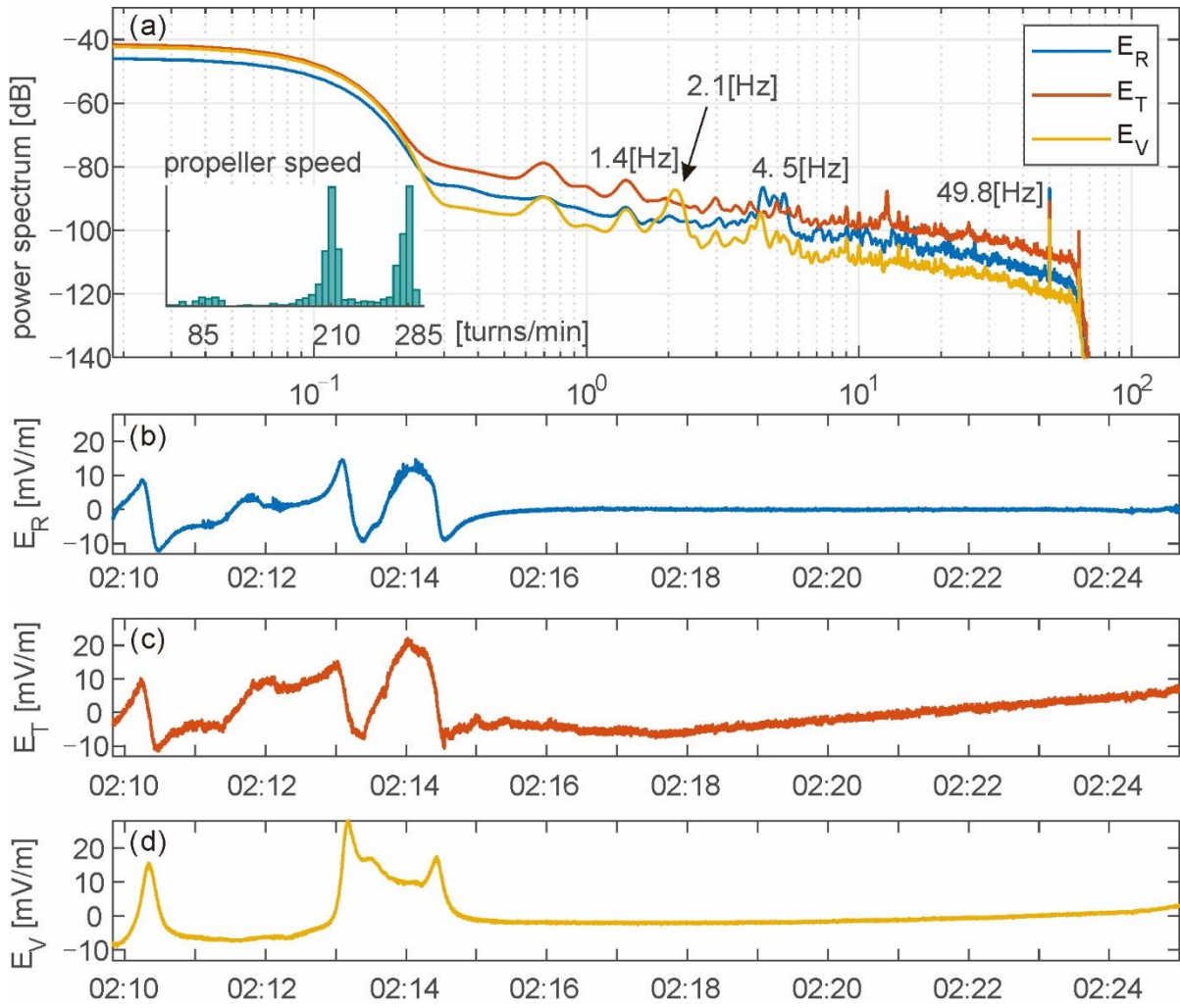
Figure 4 Time series of three components of electric field and frequency analysis of recorded data. (a) Spectrum of three components of electric field with the histogram of propeller speed, the frequency components of 1.4 Hz and 3.5-4.5 Hz are caused by the speed of propellers (b) time series of inline component E_R, (c) time series of crossline component E_T, and (d) time series of vertical component E_V.
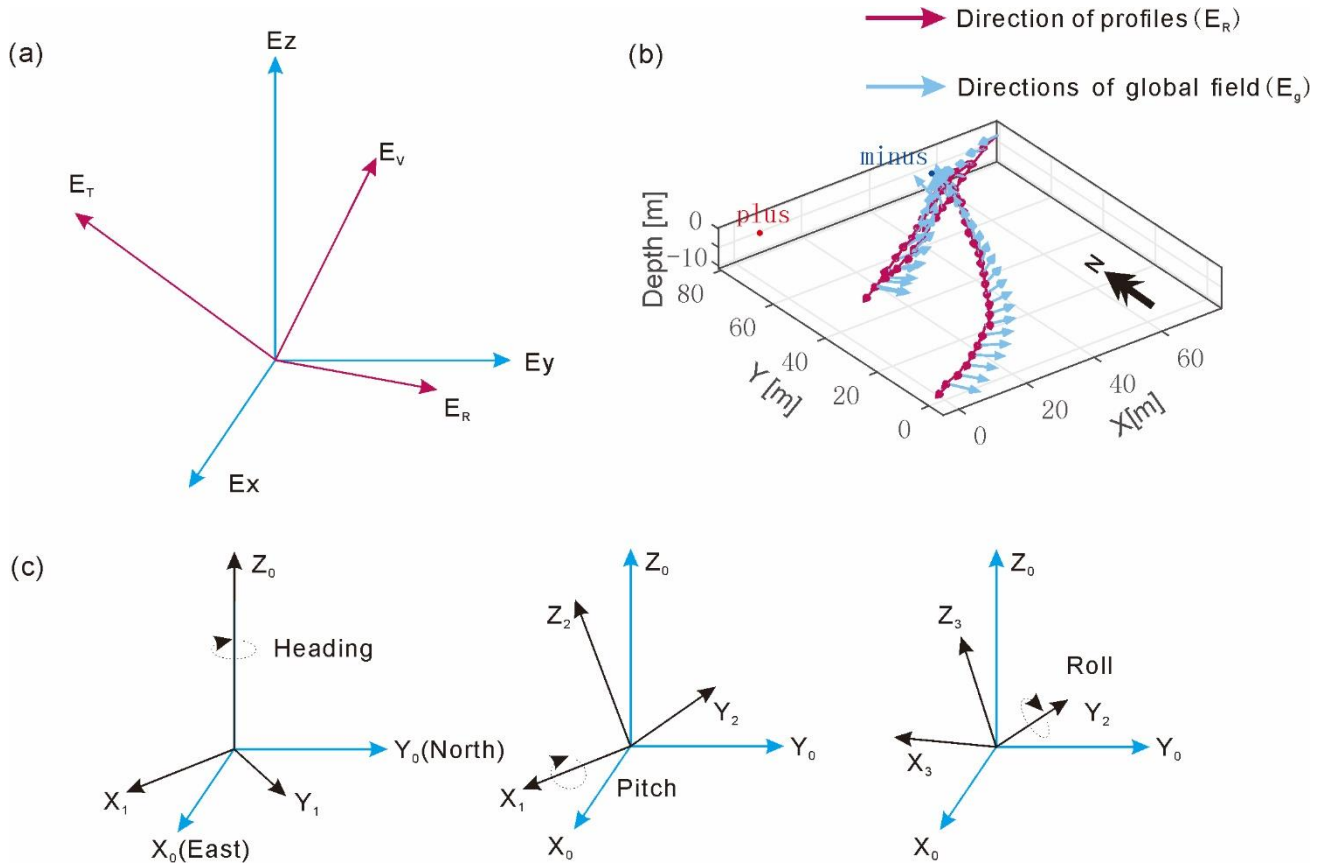
Figure 5 Rotation relationship between global electric field $\mathbf{E}_g$ and rotated electric field $\mathbf{E}_{rot}$. (a) The projection of the global and rotated electric fields in Cartesian coordinate system; (b) path of AUV in water, arrows denote the direction of AUV moving and vector direction of total electric field in geodetic coordinate system, plus denote the position of positive pole, minus denote the position of negative pole; (c) definition of different attitude angles.
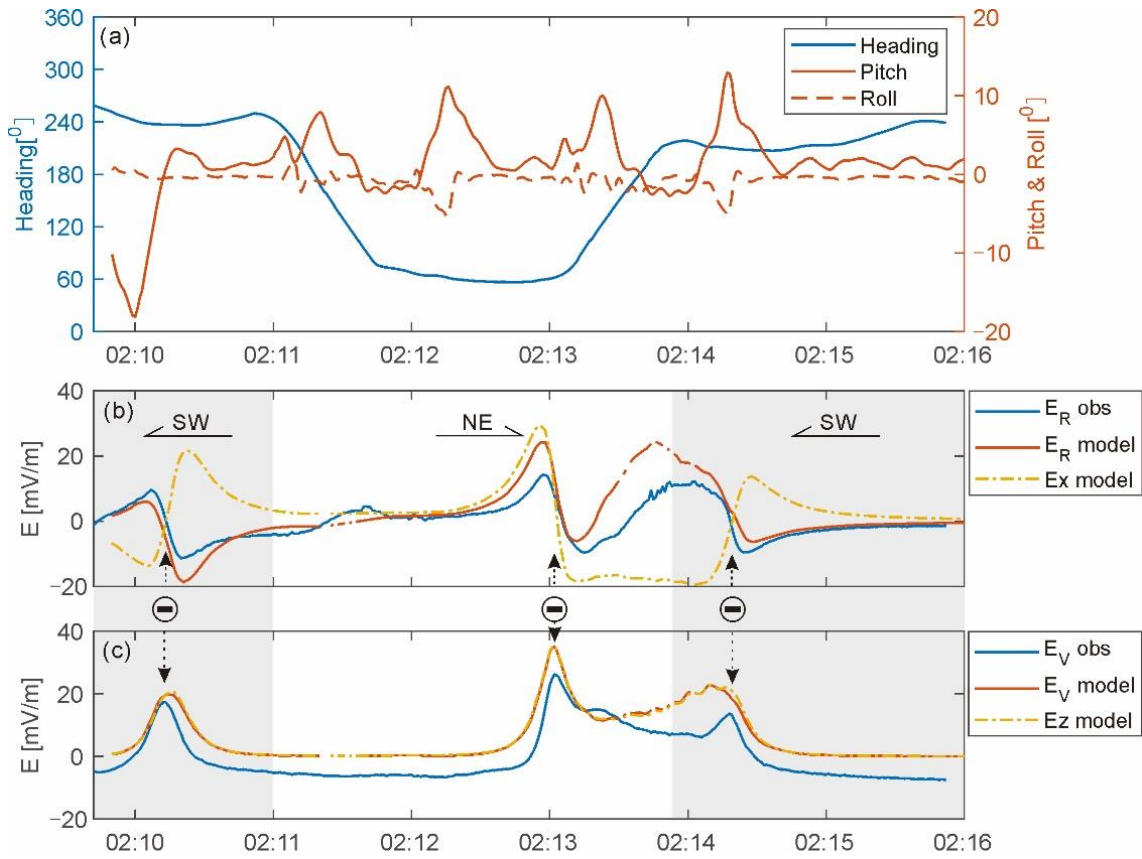
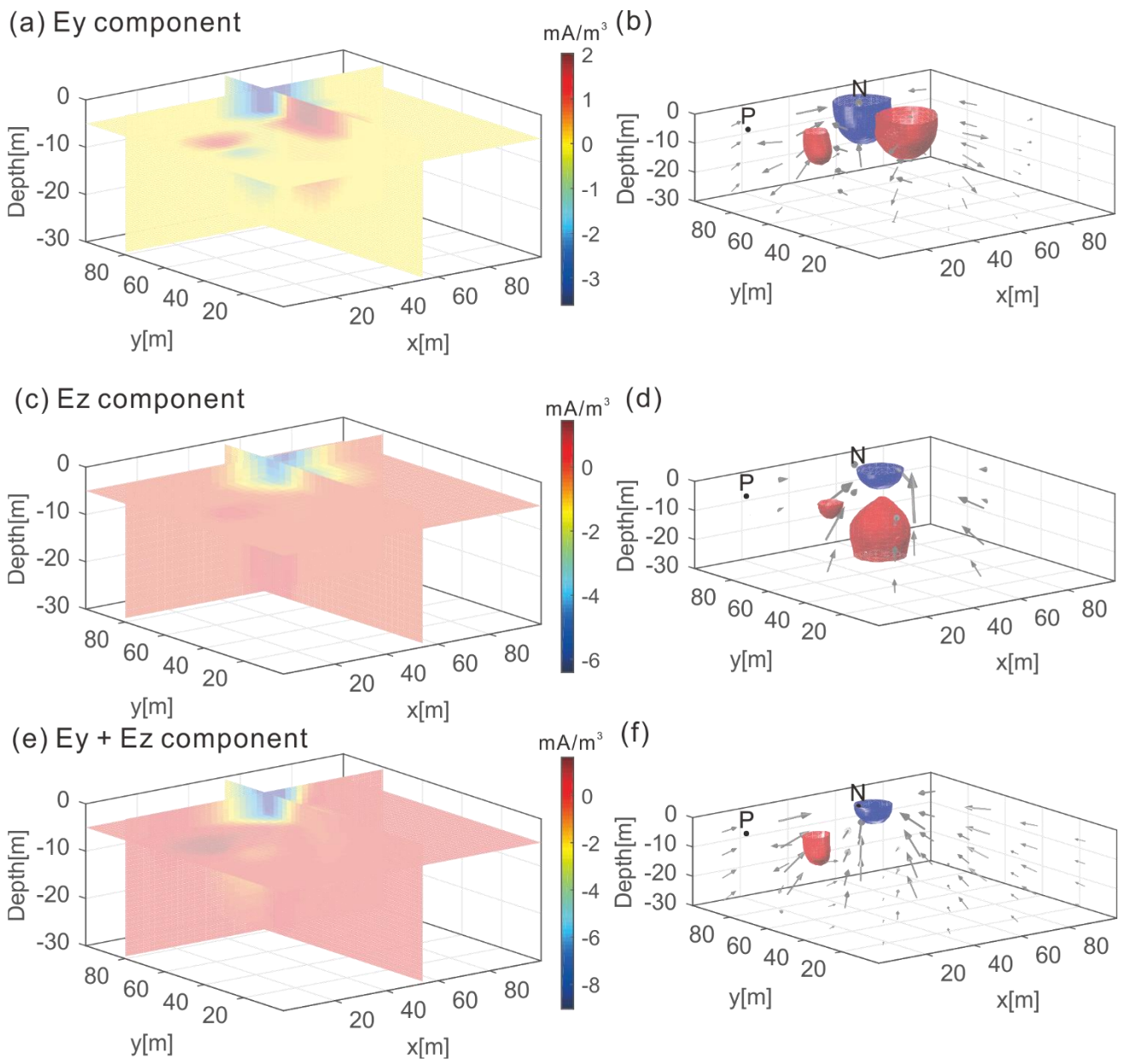**Figure 6** Comparison of the measured data and numerical simulation. (a) Navigation attitude of AUV in the water; (b) time serious of modelling and observed horizontal component with different travel direction; (c) modelling and observed vertical component for SW-NE-SW profiles. Minus corresponds to the location of negative pole of the artificial source.

Figure 7 Volumetric current density inversion results of different components of observed data, with p = 1 and α=0.01 (a) and (b) Inversion results of volumetric current density of horizontal components of electric field data (magnitude and direction), (c) and (d) Inversion results of charge density of vertical component of observed data (magnitude and direction). (e) and (f) Inversion results of charge density of both two component of observed data (magnitude and direction). The arrow direction indicates the diffusion direction of the current density. The intersection of the vertical section is the position of the negative pole of the artificial source. Although the anomaly recovery for single component can also localize the negative pole, two component inversion returns a single and compact current density. The notation P corresponds to the location of positive pole of the artificial source. The notation N corresponds to the location of negative pole.